PCCP

ROYAL SOCIETY OF CHEMISTRY

PAPER

View Article Online
View Journal | View Issue

Cite this: *Phys. Chem. Chem. Phys.*, 2025, **27**, 8121

VUV threshold photoelectron spectroscopy of SiS†

Myriam Drissi, *[a] Jean-Christophe Loison, *[b] Bérenger Gans, [c] Séverine Boyé-Péronne, [c] Hai-Linh Le, [c] Mengxu Jiang, [c] Laurent Nahon [a] and Gustavo A. Garcia [a]

Received 6th February 2025,
Accepted 25th March 2025

DOI: 10.1039/d5cp00494b

rsc.li/pccp

Silicon monosulfide (SiS) is an important molecule in astrochemistry likely linked to dust production through the formation of sulfide particles. This work presents the vacuum ultraviolet photoionisation of SiS formed *in situ* in a discharge flow reactor, in particular the threshold photoelectron spectrum covering the first three electronic states of the SiS^+ cation. The rich vibronic structure is assigned with the support of *ab initio* calculations and a spin orbit coupling constant of -323 ± 41 cm^{-1} is measured for the ground state. Adiabatic ionisation energies (10.453 ± 0.003, 10.515 ± 0.003 and 13.802 ± 0.003 eV for the ground, first and second excited state, respectively) and vibrational frequencies are also extracted from the spectra, and combined with the existing thermochemical values yields the SiS^+ dissociation energy (4.09 ± 0.01 eV).

1. Introduction

Silicon monosulfide (SiS) is an important molecule in astrochemistry which has been proposed as a precursor of sulfide grains, either by direct nucleation and/or *via* reactions leading to metal sulfides, which are a known component of dust.[1–4] In particular, an observational study in the circumstellar envelopes of carbon-rich asymptotic giant branch stars pointed SiS as a good candidate to act as a gas phase precursor of dust.[2] However, more constraints on its abundance distribution are needed to confirm this hypothesis. This requires establishing the relative importance of all possible processes including condensation onto grains and the chemical and photochemical reactivity.

In this context, modelling the abundance of SiS and SiS^+ in VUV-irradiated environments necessitates accurate ionisation energies (IEs) and dissociation thresholds, as well as spectroscopic information, while the latter can also be of interest for benchmarking theoretical methods and identifying and quantifying reaction products in laboratory experiments.[5]

Due to the experimental challenges linked to the *in situ* production of the SiS molecule, there exists only a single measurement of its photoelectron spectrum (PES), yielding an adiabatic ionisation energy (AIE) of 10.38 ± 0.02 eV.[6] However, SiS was produced in an oven at a temperature of 1200 K along with other side products, resulting in broad and overlapping bands that reduced the measurements accuracy. In addition, the contributions from impurities had to be subtracted. The electronic spectrum of SiS has also been studied theoretically, providing the IEs[7] and spectroscopic constants for its low-lying states.[7,8] These calculations predict a spin orbit splitting in the ground state of SiS^+ of -365 cm^{-1}.[8] The present work provides the threshold photoelectron spectrum of pure SiS covering ionisations from the three outermost molecular orbitals (8σ, 9σ, 3π) to improve the accuracy of existing thermochemical values and spectroscopic constants with the support of *ab initio* calculations.

2. Methodologies

2.1. Experimental

The experiments were performed at the synchrotron SOLEIL on the undulator-based DESIRS beamline.[9] The molecule of interest was produced by combining a microwave (MW) discharge with a flow-tube reactor. This setup has been described in detail elsewhere and will be only outlined briefly here.[10] The flow-tube is composed of a main tube reactor and a collinear sliding injector. The fluorine atoms are produced by MW discharge of a mixture of F_2 (Air liquide 5% in He) and He (Air liquide 99.995%) which is then fed into the main reactor, while the precursors SiH_4 (Messer 0.8% in He) and H_2S (air liquide 99.5%) enter through the injector. The position of the injector relative to the end of the reactor defines the reaction time.

[a] *Synchrotron SOLEIL, LOrme des Merisiers, St. Aubin BP 48, 91192 Gif sur Yvette, France. E-mail: myriam.drissi@synchrotron-soleil.fr*
[b] *Institut des Sciences Moléculaires (ISM), CNRS, Univ. Bordeaux, 351 cours de la Libération, Talence, 33400, France. E-mail: jean-christophe.loison@cnrs.fr*
[c] *Institut des Sciences Moléculaires dOrsay (ISMO), CNRS, Université Paris-Saclay, 91405 Orsay, France*

† Electronic supplementary information (ESI) available. See DOI: https://doi.org/10.1039/d5cp00494b

The total pressure in the reactor is 3.5×10^{-3} mbar for a total flow of around 1000 sccm (standard cubic centimeter per minute). The concentrations of fluorine, silane and hydrogen sulfide are estimated to be around 2×10^{13}, 1×10^{13} and 2×10^{13} cm^{-3} respectively. The F atoms can react with the precursors by successive H-abstraction reactions to generate SiH_x (x = 0–3) and H_yS (y = 0–1). These molecules may react together as well, producing a wide variety of species. The experimental conditions, including precursors concentration and injector distance, are optimised for the production of SiS. The gas mixture from the reactor is skimmed twice[11] before entering the interaction chamber to cross the VUV beam with a right angle in the center of the double imaging photoelectron/photoion spectrometer DELICIOUS III.[12] The beamline is set to provide a monochromatized, linearly polarized light. A gas filter,[13] located upstream the monochromator, is filled with argon to ensure a high spectral purity by cutting off the harmonics from the undulator spectrum.

After interaction with the VUV beam, the resulting electrons and ions are accelerated in opposite directions by an electric DC field of F = 44 V cm^{-1} towards a velocity map imaging (VMI) and an imaging linear time-of-flight (iTOF) detector, respectively. This extraction field induces a downshift of the ionisation energies of 5 meV, following the well-established formula $6\sqrt{F}$ (cm^{-1}).[14] All values given below were therefore shifted up accordingly. The data were recorded in a double imaging photoelectron-photoion coincidence (i^{2}PEPICO) acquisition scheme. This allows the simultaneous recording of mass-selected photoelectron images from which photoelectron spectra can be extracted for each mass, and at each photon energy by Abel transform.[15] The threshold photoelectron signal is obtained by integrating along constant ionic state lines up to an electron kinetic energy of 20 meV, according to a previously described methodology.[16]

The spectra were recorded by scanning the photon energy in the 9.9 to 11.2 eV and 13.4 to 14.5 eV intervals with a 5 meV step, and were normalised by the recorded photon flux. A loss of about 30% of signal over a few hours could be noticed, and attributed to the polymerisation of the reactants leading to skimmer clogging. This effect was corrected by recording a fast scan with larger energy step, for which the conditions were stable over time, as previously described.[17]

The absolute energy calibration was achieved with the HS and atomic sulfur ionisation energies as well as sulfur autoionisation absorptions between 10.59 and 10.73 eV for the first energy range, and with Ar $3p^5$ 3d (3/2) and $3p^5$ 3d (1/2) absorption lines from the gas filter and the ionisation energy of the S atom ($3s^23p^3[^2P_{1/2}{}^0]$ final ion state) for the second energy range. This led to an absolute energy scale accuracy of 2.5 meV over the full range. The photon resolution was 0.72 Å (6 meV at 10 eV and 11 meV at 13.5 eV) for both scans. The total (electron + photon) energy resolution was 13 meV and 14 meV for the lower and higher energy scans, respectively, as measured from the atomic signals.

The ion image was used to select only ions possessing a velocity component along the molecular axis, therefore discarding contribution from the ionisation chamber background (as previously described[10]). Furthermore, the ion image analysis provided an estimation of the translational temperature of around 240 K, which is assumed equal to the rotational temperature.[18]

2.2. Computational

The *ab initio* calculations on the electronic states of SiS and SiS^+ were carried out using first the internally contracted multireference configuration interaction method with Davidson correction (MRCI + Q) with complete active space self-consistent field (CASSCF) wavefunctions, and also using the coupled cluster method (R)CCSD(T). The CASSCF and MRCI calculations were performed at full valence, namely with 10 (9 for SiS^+) electrons distributed in 8 orbitals with the 1s, 2s and 2p orbitals of silicon and sulfur atoms kept doubly occupied. All calculations were performed using the MOLPRO 2015 package.[19] Single point calculations were performed with the AVnZ (n = T, Q, 5, and 6) basis set for the equilibrium geometries and anharmonic frequencies (using the DIATOMIC routine in MOLPRO where the potential curves were fitted with a polynomial of 10th order, allowing the spectroscopic constants to be calculated (ω_e, $\omega_e x_e$, and $\omega_e y_e$)). The spin–orbit matrix elements and eigenstates were computed at MRCI level using the Breit-Pauli (BP) operator. Complete basis set (CBS) extrapolations were carried out using the AVnZ (n = T, Q, 5, and 6) basis set series. For CASSCF/MRCI calculations the CASSCF and dynamical correlation ($E_{MRCI+Q} - E_{CASSCF}$) energies were extrapolated using the $E_{CASSCF}(CBS) + A \times e^{-Bn}$ and $E_{Corr}(CBS) + C \times n^{-3}$ functions, respectively. The calculated energies reported in this paper correspond to $E_{CASSCF}(CBS) + E_{Corr}(CBS)$. For (R)CCSD(T) calculations the energies were extrapolated using $E_{Corr}(CBS) + C \times n^{-3}$ function. At the MRCI and CCSD(T) levels, the equilibrium distances were extrapolated using the expression $r_e(CBS) + C \times n^{-3}$ function. The anharmonic constants ($\omega_e x_e$, and $\omega_e y_e$) could not be extrapolated because their trend could not be fitted. Indeed, the values depend slightly on the basis used (*i.e.* without regular progression) and here it was preferred to keep the values obtained with the largest basis set (AV6Z). It should be noted that the second $B^{+2}\Sigma^+$ state cannot be calculated at CCSD(T) level because only the first state of a given symmetry can be calculated using this method. Therefore, only the values calculated at MRCI level are reported in Table 1 for this state.

The Franck–Condon (FC) calculations presented in this study were performed using the ezSpectrum software,[20] with *ab initio* MOLPRO output files generated using the AV6Z basis set for all states. The simulations were scaled by estimating the relative partial ionisation cross sections of SiS and considering the experimental resolution. A vibrational temperature of 1000 K was considered for the Franck–Condon harmonic simulation. Note that in threshold photoelectron spectroscopy, autoionisation might affect vibrational branching ratios[21] so that the chosen temperature should be taken as an estimate that best fits the experimental spectrum.

3. Results and discussion

3.1. Composition of the reactor

The mass spectrum obtained from the integration of the TOF between 9.9 and 10.9 eV for the SiH_4 + H_2S + F system is

Table 1 Experimental and calculated ionisation energies of SiS and spectroscopic constants for the $X^+\ ^2\Pi_{3/2}$, $X^+\ ^2\Pi_{1/2}$, $A^+\ ^2\Sigma^+$ and $B^+\ ^2\Sigma^+$ states of SiS^+

State	T_e (cm^{-1})	r_e (Å)	ω_e (cm^{-1})	$\omega_e x_e$ (cm^{-1})	IE (eV)	Ref.
$X^+\ ^2\Pi_{3/2}$	**83 999 ± 30**		**635 ± 30**		**10.453 ± 0.003**	**Exp**
		2.065	**595.23**	**2.50**	**10.365**	**Calc MRCI**
		2.066	**601.18**	**2.20**	**10.440**	**Calc CCSD(T)**
		2.05 ± 0.01	700 ± 30		10.38 ± 0.02	Exp.[a 6]
		2.085	576		10.2	Calc.[8]
		3.936	547.2*		10.43	Calc.[b 7]
$X^+\ ^2\Pi_{1/2}$	**84 338 ± 20**		**597 ± 28**		**10.493 ± 0.003**	**Exp**
		2.065	**595.23**	**2.50**	**10.403**	**Calc MRCI**
		2.066	**601.18**	**2.20**	**10.478**	**Calc CCSD(T)**
		2.087	576	2.50	10.35	Calc[8]
$A^+\ ^2\Sigma^+$					**10.515 ± 0.003**	**Exp**
		1.917	**720.88**	**3.32**	**10.661**	**Calc MRCI**
		1.918	**729.26**	**2.34**	**10.517**	**Calc CCSD(T)**
					10.53 ± 0.02	Exp[6]
		1.934	704		10.35	Calc[8]
$B^+\ ^2\Sigma^+$	**111 050 ± 37**		**551 ± 45**		**13.802 ± 0.003**	**Exp**
		2.017	**572.15**	**4.57**	**13.660**	**Calc MRCI**
		2.05 ± 0.01	655 ± 30		13.73 ± 0.03	Exp.[6]
		2.048	535		13.55	Calc.[8]

Values from this work are in bold. [a] The spin–orbit splitting was not resolved in this experiment. [b] The spin–orbit coupling was not taken into account in the calculations. Calculations with MP2 level of theory except for * which was calculated with HF.

presented in Fig. 1. This integration range was selected to remain below the SiH_4 ionisation energy (about 11 eV) for clarity since it overlaps with the ^{32}S atom peak in our mass spectra.

Under these experimental conditions, the SiS molecule was produced efficiently, with a good signal-to-noise ratio (SNR) compared to the precursors. Its formation can occur through several possible pathways, including S + SiH, S_2 + SiH, or SH + SiH, all of which have been reported as exothermic in the literature.[22–24] Beyond *m*/*z* 60, numerous heavier molecules with masses up to *m*/*z* 256 amu were also detected, as seen in Fig. S5 and S6 of the ESI.† These species do not interfere with the molecule of interest due to the selectivity of the PEPICO technique, as mentioned previously. Moreover, the sharp TOF peaks indicate ions formed from genuine neutral species, excluding the possibility of contribution from fragments.

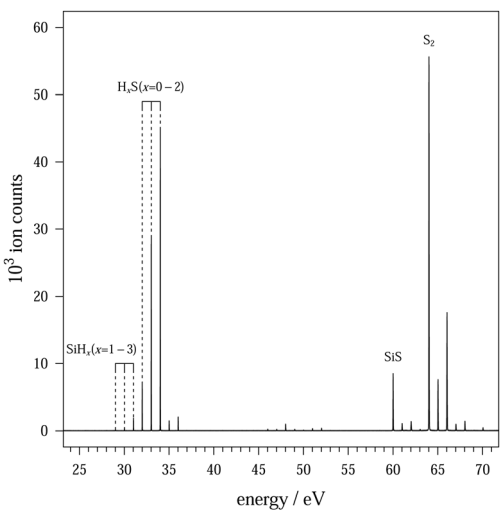

Fig. 1 TOF mass spectra integrated between 9.9 and 10.9 eV photon energy for the F + SiH_4 + H_2S system.

3.2. Threshold photoelectron spectra

The mass-selected threshold photoelectron spectra (TPES) at *m*/*z* 60 are shown in Fig. 2 over two photon energy ranges: 9.9–11.2 eV and 13.5–14.5 eV, along with the simulated spectra. They correspond to three ionising transitions originating from the $X\ ^1\Sigma^+$ ground state of SiS. Note that the corresponding ion yields are available in supplementary note 1 (Fig. S1 and S2, ESI†).

The spectrum corresponding to the 9.9–11.2 eV energy region is shown in Fig. 3. Two overlapping bands could be assigned to the $X^+\ ^2\Pi \leftarrow X\ ^1\Sigma^+$ and $A^+\ ^2\Sigma^+ \leftarrow X\ ^1\Sigma^+$ ionising transitions. Several hot bands and sequence bands could be

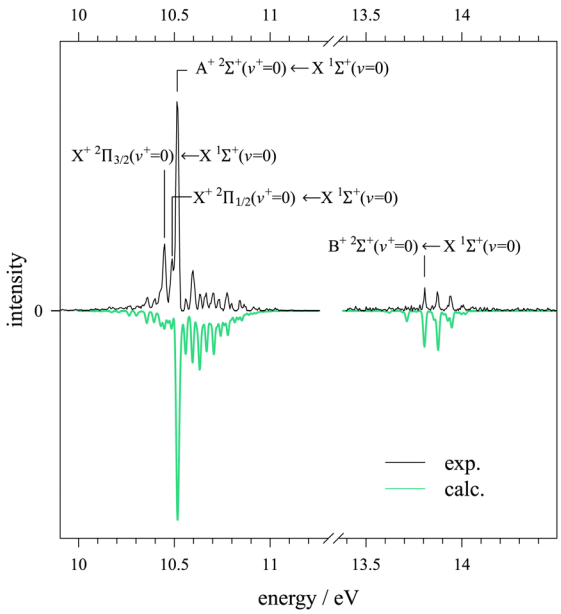

Fig. 2 Experimental TPES of SiS (black trace) in comparison with Franck–Condon simulations (green trace) in both 9.9–11.2 and 13.5–14.5 eV energy ranges. See text for details.

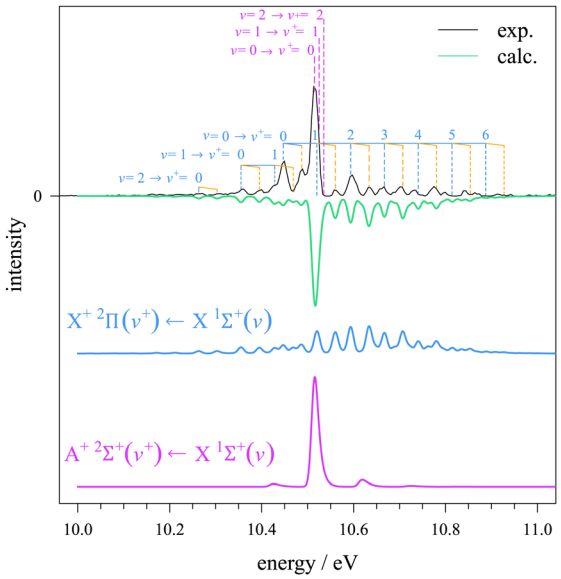

Fig. 3 Mass-selected experimental TPES of SiS in the vicinity of $X^+\ ^2\Pi \leftarrow X\ ^1\Sigma^+$ and $A^+\ ^2\Sigma^+ \leftarrow X\ ^1\Sigma^+$ ionising transitions (black trace). The Franck–Condon simulation for the individual $X^+\ ^2\Pi$ and $A^+\ ^2\Sigma$ are shown in blue and pink respectively. The sum of both is plotted in green in comparison with the black experimental trace. The $X^+\ ^2\Pi_{3/2}$ corresponds to the blue dashed line while the $X^+\ ^2\Pi_{1/2}$ corresponds to the orange one. The simulation for the ground state includes the calculated spin–orbit coupling constant of $-304.36\ cm^{-1}$. See text for details.

also identified, originating from $v = 1$ and $v = 2$ vibrational states of the neutral, arising from the exothermicity of H abstraction reactions which leads to vibrationally and even electronically excited neutral species in the reactor.[25] The spin–orbit splitting of the $X^+\ ^2\Pi$ state could be resolved, leading to the assignment of the $X^+\ ^2\Pi_{3/2}$ and $X^+\ ^2\Pi_{1/2}$ states, both exhibiting a clear vibrational structure.

For the $X^+\ ^2\Pi$ state, precise measurements of the adiabatic ionisation energies (AIE) of both spin components were obtained as 10.453 ± 0.003 eV and 10.493 ± 0.003 eV, respectively. These values are in good agreement with the calculations in this work (Table 1) but are slightly higher than those reported in previous experimental and theoretical studies.[6–8] The earlier experimental work by Cockett *et al.*[6] was conducted at high temperatures (~1200 K) using a pyrolysis oven, leading to broad and overlapping spectral lines that affected the measured IE. Consequently, the two spin components could not be resolved, and the (0, 0) transition overlapped with hot bands. In contrast, the present spectrum clearly distinguishes the (0, 0) transition, resulting in a more robust measurement of the AIE. The dissociation energy (D_0^0) of $X^+\ ^2\Pi_{3/2}$ can be derived under the assumption that $SiS(X\ ^1\Sigma^+)$ dissociates into $Si(^3P_0)$ and $S(^3P_2)$, while $SiS^+(X^+\ ^2\Pi_{3/2})$ dissociates into $Si^+(^2P_{1/2})$ and $S(^3P_2)$. The dissociation energy of $SiS(X\ ^1\Sigma^+)$ was measured to be 6.39 ± 0.13 eV,[26] and the ionisation energy of the Si atom was determined to be 8.15168 ± 0.00003 eV.[27] Using the updated IE of SiS, this yields a D_0^0 value of 4.09 ± 0.01 eV through the Born–Haber cycle. Note that the precision of the dissociation energy of the cation SiS^+ is ultimately limited here by the uncertainty of the dissociation energy of the neutral SiS.

The simulation is found to reproduce well the spectrum except for the intensity of the (0, 0) transition of both spin components which appears more intense than predicted. Although the discrepancy could be due to the accuracy of the calculated equilibrium distances, it likely stems from autoionisation resonances affecting the shape of the TPES due to their large cross-sections and potentially different wavefunction overlaps to the final state. Indeed, such autoionisation processes have been used to map regions of the cation molecular potential that are not accessible by direct ionisation.[28] The contribution from direct and indirect ionisation can be distinguished by comparing different integration regions, as demonstrated in the case of coronene.[29] For similar integration regions, partial cross-sections are not expected to change since they vary smoothly, within eVs, while the autoionisation signal will vary rather sharply.

Supplementary notes 1–3 (ESI†) show the ion yield, a comparison between two integration regions to obtain the TPES from the PES matrix and the full PES matrix, respectively. Although the ion yield does not show evidence of autoionisations, perhaps due to their short lifetimes, the dependence of the vibrational branching ratios on the electron energy integration interval points to their presence, while the PES matrix in Fig. S4 (ESI†) clearly shows an enhanced intensity in the constant ionic state corresponding to $X^+\ ^2\Pi(\nu^+ = 0) \leftarrow X\ ^1\Sigma^+(\nu = 0)$ ending abruptly at the threshold of the $A^+\ ^2\Sigma^+$, related to Rydberg series converging towards this state.

The average experimental spin–orbit splitting of $-323 \pm 41\ cm^{-1}$ was found between the two $X^+\ ^2\Pi$ components. The uncertainty is given within 2σ. It appears in reasonable agreement with the previous calculation of $-365\ cm^{-1}$ (ref. 8) and is fully consistent with the present calculated value of $-304.36\ cm^{-1}$.

The first excited $A^+\ ^2\Sigma^+$ state shows a vibrational structure dominated by the adiabatic transition and the $\nu^+ = 1 \leftarrow \nu = 0$ ionising transition to the $X^+\ ^2\Pi_{3/2}$ state. Sequence bands transitions to the $A^+\ ^2\Sigma^+$ state ($\nu^+ = 1 \leftarrow \nu = 1$ and $\nu^+ = 2 \leftarrow \nu = 2$) may also contribute to the non-symmetric profile of the line. With the help of the calculated spectrum, the adiabatic transition could be assigned at 10.515 ± 0.003 eV. This value is consistent with the previous measurement of 10.53 ± 0.02 eV,[6] and agrees well with the calculated IE at 10.517 eV from this work using CCSD(T) method.

The higher energy spectrum between 13.5–14.5 eV is presented in Fig. 4, which includes the $B^+\ ^2\Sigma^+ \leftarrow X\ ^1\Sigma^+$ transition up to $\nu^+ = 3$ as well as two hot bands originated from the $\nu = 1$ and $\nu = 2$ of the $X\ ^1\Sigma^+$ neutral state. An experimental value of 13.802 ± 0.003 eV was found for the AIE, which compares well with the calculation performed in this work (Table 1). There is overall a good agreement between the simulation and the experimental spectrum barring a slight discrepancy for the intensity ratios of the hot bands owing to the inability to fit the full spectrum with a single vibrational temperature, most likely due to the effect of autoionisation, as discussed for the X^+ and A^+ states.

The vibrational progression of each state was fitted to extract the spectroscopic constants according to $E = T_e + \omega_e(\nu + 1/2) - \omega_e x_e(\nu + 1/2)^2$. The results are presented in Table 1. The lines were fitted up to $\nu^+ = 4$ and $\nu^+ = 3$ for the $X^+\ ^2\Pi$ and $B^+\ ^2\Sigma^+$ states,

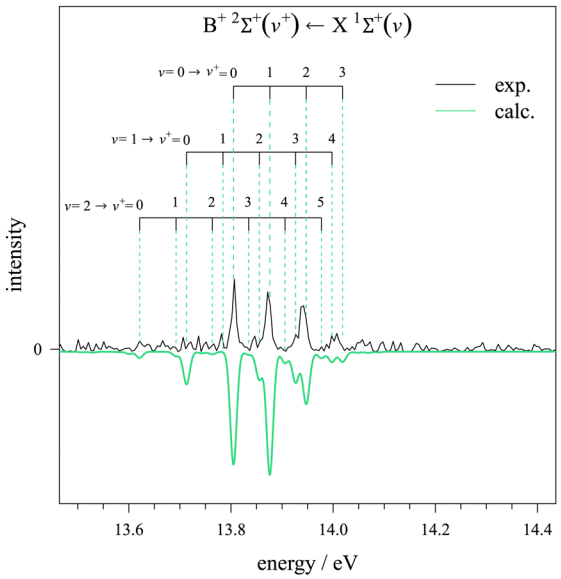

Fig. 4 Mass-selected experimental TPES of SiS in the vicinity of $B^+\ ^2\Sigma^+ \leftarrow X\ ^1\Sigma^+$ transition (black trace) compared to Franck–Condon simulations (green trace).

respectively, as the signal was too weak afterwards. For the $X^+\ ^2\Pi_{3/2}$ state, the $v^+ = 1$ line could not be fitted as it overlaps with the $A^+\ ^2\Sigma^+$ state. The anharmonicity constant, denoted by $\omega_e x_e$, could not be extracted from the experimental data due to the limited number of lines available for analysis. Note that through theoretical calculations, the value of $\omega_e x_e$ was found to be smaller than 5 cm^{-1} for all states, well below our experimental precision.

Overall, the values of ω_e and the computed r_e are found to be consistent with the available literature, although slightly higher values of ω_e were observed by Cockett *et al.*[6] The transitions energies within the cation states can be deduced and compared with the values computed by Chattopadhyaya and Das[8] by subtracting the different IE of the excited state with the ground state $X^+\ ^2\Pi_{3/2}$. The energy difference with the $X^+\ ^2\Pi_{1/2}$ and $B^+\ ^2\Sigma^+$ states shows excellent agreement, with experimental values of 322 cm^{-1} (0.040 eV) and 27 011 cm^{-1} (3.349 eV), compared to the computed values of 365 cm^{-1} (0.045 eV) and 27 113 cm^{-1} (3.361 eV), respectively. In contrast, the $A^+\ ^2\Sigma^+$ state exhibits a larger discrepancy, with an experimental value of 540 cm^{-1} (0.067 eV) compared to the computed 1203 cm^{-1} (0.149 eV).

Conclusions

The silicon monosulfide photoelectron spectrum comprising transitions to the ground and first two excited electronic states of the cation has been recorded using a double imaging photoelectron-photoion spectrometer in conjunction with synchrotron radiation. The radical was produced by successive H abstractions of two precursors, silane and hydrogen sulfide, which can further react in a flow tube reactor. Comparison to *ab initio* calculations allowed the assignment of the vibronic transitions yielding spectroscopic constants for the ground and second excited state of the cation, including the spin–orbit splitting value of the ground state. This provides a refined measurement of the adiabatic ionisation energies as well as an updated dissociation energy in the ground state of the cation. The photoelectron spectrum in this work acts as a fingerprint that can be used to detect SiS by advanced mass spectrometry[5] in gas phase reaction studies, and can also provide the foundation for recording laser-based, high-resolution zero kinetic energy (ZEKE) spectra, suitable for identifying molecules in space, as recently exemplified by the detection of CH_3^+.[30]

Data availability

Data supporting this article have been included as part of the ESI.† Raw data are available from the corresponding authors, upon reasonable request.

Conflicts of interest

There are no conflicts to declare.

Acknowledgements

This work has received financial support from the French "Agence Nationale de la Recherche" (ANR) under Grant No. ANR-21-CE29-0017 (Project ZEPHIRS). This work was performed on the DESIRS beamline at the SOLEIL synchrotron under Proposals No. 20240446 and 99240021. We are grateful to the whole staff at SOLEIL for smoothly running the facility, in particular the beamline staff Nelson De Oliveira and Jean-François Gil for their precious help in performing the experiments.

Notes and references

1 I. Cherchneff, *Astron. Astrophys.*, 2006, **456**, 1001–1012.
2 S. Massalkhi, M. Agúndez and J. Cernicharo, *Astron. Astrophys.*, 2019, **628**, A62.
3 K. Smolders, P. Neyskens, J. A. D. L. Blommaert, S. Hony, H. V. Winckel, L. Decin, S. V. Eck, G. C. Sloan, J. Cami, S. Uttenthaler, P. Degroote, D. Barry, M. Feast, M. A. T. Groenewegen, M. Matsuura, J. Menzies, R. Sahai, J. T. V. Loon, A. A. Zijlstra, B. Acke, S. Bloemen, N. Cox, P. D. Cat, M. Desmet, K. Exter, D. Ladjal, R. Østensen, S. Saesen, F. V. Wyk, T. Verhoelst and W. Zima, *Astron. Astrophys.*, 2012, **540**, A72.
4 S. Zhukovska and H.-P. Gail, *Astron. Astrophys.*, 2008, **486**, 229–237.
5 I. Fischer and S. T. Pratt, *Phys. Chem. Chem. Phys.*, 2022, **24**, 1944–1959.
6 M. C. R. Cockett, J. M. Dyke, A. Morris and M. H. Z. Niavaran, *J. Chem. Soc., Faraday Trans. 2*, 1989, **85**, 75–83.
7 P. J. Bruna and F. Grein, *J. Phys. Chem.*, 1992, **96**, 6617–6623.
8 S. Chattopadhyaya and K. K. Das, *J. Phys. B: At., Mol. Opt. Phys.*, 2004, **37**, 3355–3367.
9 L. Nahon, N. De Oliveira, G. A. Garcia, J.-F. Gil, B. Pilette, O. Marcouillé, B. Lagarde and F. Polack, *J. Synchrotron Radiat.*, 2012, **19**, 508–520.

10 G. A. Garcia, X. Tang, J.-F. Gil, L. Nahon, M. Ward, S. Batut, C. Fittschen, C. A. Taatjes, D. L. Osborn and J.-C. Loison, *J. Chem. Phys.*, 2015, **142**, 164201.
11 X. Tang, G. A. Garcia, J.-F. Gil and L. Nahon, *Rev. Sci. Instrum.*, 2015, **86**, 123108.
12 G. A. Garcia, B. K. Cunha de Miranda, M. Tia, S. Daly and L. Nahon, *Rev. Sci. Instrum.*, 2013, **84**, 053112.
13 B. Mercier, M. Compin, C. Prevost, G. Bellec, R. Thissen, O. Dutuit and L. Nahon, *J. Vac. Sci. Technol., A*, 2000, **18**, 2533–2541.
14 W. A. Chupka, *J. Chem. Phys.*, 1993, **98**, 4520–4530.
15 G. A. Garcia, L. Nahon and I. Powis, *Rev. Sci. Instrum.*, 2004, **75**, 4989–4996.
16 J. C. Poully, J. P. Schermann, N. Nieuwjaer, F. Lecomte, G. Grégoire, C. Desfrançois, G. A. Garcia, L. Nahon, D. Nandi, L. Poisson and M. Hochlaf, *Phys. Chem. Chem. Phys.*, 2010, **12**, 3566.
17 H. R. Hrodmarsson, G. A. Garcia, H. Linnartz and L. Nahon, *Phys. Chem. Chem. Phys.*, 2020, **22**, 13880–13892.
18 G. A. Garcia, B. Gans, X. Tang, M. Ward, S. Batut, L. Nahon, C. Fittschen and J.-C. Loison, *J. Electron Spectrosc. Relat. Phenom.*, 2015, **203**, 25–30.
19 H.-J. Werner, P. J. Knowles, P. Celani, W. Györffy, A. Hesselmann, D. Kats, G. Knizia, A. Köhn, T. Korona, D. Kreplin, R. Lindh, Q. Ma, F. R. Manby, A. Mitrushenkov, G. Rauhut, M. Schütz, K. R. Shamasundar, T. B. Adler, R. D. Amos, S. J. Bennie, A. Bernhardsson, A. Berning, J. A. Black, P. J. Bygrave, R. Cimiraglia, D. L. Cooper, D. Coughtrie, M. J. O. Deegan, A. J. Dobbyn, K. Doll, M. Dornbach, F. Eckert, S. Erfort, E. Goll, C. Hampel, G. Hetzer, J. G. Hill, M. Hodges, T. Hrenar, G. Jansen, C. Köppl, C. Kollmar, S. J. R. Lee, Y. Liu, A. W. Lloyd, R. A. Mata, A. J. May, B. Mussard, S. J. McNicholas, W. Meyer, T. F. Miller III, M. E. Mura, A. Nicklass, D. P. O'Neill, P. Palmieri, D. Peng, K. A. Peterson, K. Pflüger, R. Pitzer, I. Polyak, M. Reiher, J. O. Richardson, J. B. Robinson, B. Schröder, M. Schwilk, T. Shiozaki, M. Sibaev, H. Stoll, A. J. Stone, R. Tarroni, T. Thorsteinsson, J. Toulouse, M. Wang, M. Welborn and B. Ziegler, *MOLPRO, version, a package of ab initio programs*, see **https://www.molpro.net**.
20 S. Gozem and A. I. Krylov, *WIREs Comput. Mol. Sci.*, 2022, **12**, e1546.
21 P.-M. Guyon, R. Spohr, W. A. Chupka and J. Berkowitz, *J. Chem. Phys.*, 1976, **65**, 1650–1658.
22 B. R. L. Galvão, P. J. S. B. Caridade, V. C. Mota and A. J. C. Varandas, *Mon. Not. R. Astron. Soc.*, 2023, **525**, 5353–5358.
23 M. Rosi, L. Mancini, D. Skouteris, C. Ceccarelli, N. Faginas Lago, L. Podio, C. Codella, B. Lefloch and N. Balucani, *Chem. Phys. Lett.*, 2018, **695**, 87–93.
24 R. C. Fortenberry and B. A. McGuire, *Astrophys. J.*, 2024, **971**, 101.
25 H. R. Hrodmarsson, G. A. Garcia, L. Nahon, J.-C. Loison and B. Gans, *Phys. Chem. Chem. Phys.*, 2019, **21**, 25907–25915.
26 S. J. Q. Robinson and R. F. Barrow, *Proc. Phys. Soc., London, Sect. A*, 1954, **67**, 95–96.
27 W. C. Martin and R. Zalubas, *J. Phys. Chem. Ref. Data*, 1983, **12**, 323–380.
28 M. Briant, L. Poisson, M. Hochlaf, P. De Pujo, M.-A. Gaveau and B. Soep, *Phys. Rev. Lett.*, 2012, **109**, 193401.
29 P. Bréchignac, G. A. Garcia, C. Falvo, C. Joblin, D. Kokkin, A. Bonnamy, P. Parneix, T. Pino, O. Pirali, G. Mulas and L. Nahon, *J. Chem. Phys.*, 2014, **141**, 164325.
30 P. B. Changala, N. L. Chen, H. L. Le, B. Gans, K. Steenbakkers, T. Salomon, L. Bonah, I. Schroetter, A. Canin, M.-A. Martin-Drumel, U. Jacovella, E. Dartois, S. Boyé-Péronne, C. Alcaraz, O. Asvany, S. Brünken, S. Thorwirth, S. Schlemmer, J. R. Goicoechea, G. Rouillé, A. Sidhu, R. Chown, D. Van De Putte, B. Trahin, F. Alarcón, O. Berné, E. Habart and E. Peeters, *Astron. Astrophys.*, 2023, **680**, A19.

